Journal of Sedimentary Research

Journal of Sedimentary Research, 2018, v. 88, 1–15
Research Article
DOI: http://dx.doi.org/10.2110/jsr.2019.1

SAND LIQUEFACTION INDUCED BY A BLAST TEST: NEW INSIGHTS ON SOURCE LAYER AND GRAIN-SIZE SEGREGATION MECHANISMS (LATE QUATERNARY, EMILIA, ITALY)

DANIELA FONTANA,[1] SARA AMOROSO,[2] LUCA MINARELLI,[3] AND MARCO STEFANI[4]
[1]*Department of Chemical and Geological Sciences, University of Modena and Reggio Emilia, Modena, Italy*
[2]*Istituto Nazionale di Geofisica e Vulcanologia, L'Aquila, Italy*
[3]*Geotema s.r.l., Spin-off University of Ferrara, Italy*
[4]*Department of Architecture, University of Ferrara, Italy*
e-mail: daniela.fontana@unimore.it

ABSTRACT: **The composition and texture of liquefied sands represent an important tool for the recognition of buried source layers and for a better understanding of earthquake-induced liquefaction mechanisms. The earthquake-simulating field experiment (blast test) carried out in 2016 in fluvial sediments of the Emilia plain induced subsurface liquefaction and the surface expulsion of sand as sand blows. The area was widely affected by liquefaction phenomena during the Mw 6.1 Emilia earthquake (2012). The grain size and composition of sand blows ejected during the blast test have been compared with various horizons of buried fluvial sediments as deep as 20 m, and with sands from two trenches in the blast site representative of co-seismic 2012 liquefied sands. The sands from the cores show a clear trend from shallow lithoarenitic to deeper quartz–feldspar-rich compositions. The sands at shallow depth (up to 7.7 m) are the most lithoarenitic, with fine-grained sedimentary rock fragments (shales, siltstones, and limestone) as the dominant lithic type. Lithic fragments derive mostly from erosion of sedimentary terrigenous and carbonate successions of Apenninic affinity. In contrast, deeper sands (at depth > 7.7 m) are enriched in quartz and feldspars and impoverished in lithic fragments, which are similar in character to Po River sands. The composition of ejected sands largely overlap that of the shallow litharenitic Apenninic sands, indicating that liquefaction processes affected mainly sand layers at relatively shallow depth (5.9–7.7 m). Textural parameters show that silty sands and silts characterized by relatively high content of fines can also liquefy. This is in contrasts to most of the literature, where fine-grained sediments are considered as incapable of generating the high pore pressures commonly associated with liquefaction. This result should be considered when estimating the liquefaction as a potential hazard. Moreover, we observe that there is a selective loss of fines in the clastic dikes and sand volcanoes relative to the source beds, indicating that the liquefaction process appears to preferentially select the diameters of the grains that reach the ground surface, probably following the generated excess pore-water pressure. This may have caused the segregation and dispersion of the fine silt–clay content, producing highly sorted sand boils. This effect is easlit observable in both the blast-induced sand boils, and the co-seismic 2012 dikes and sand boils ejected in the same area.**

INTRODUCTION

Extensive liquefaction phenomena of fluvial sands buried in the shallow subsurface have occurred in the central-eastern sector of the Po plain, following the two main shocks (M_L 5.8 and 5.9) of the 2012 Emilia earthquake. The ejection of liquefied sands through fractures to the surface has generated numerous sand boils, concentrated along buried old channels of Apenninic rivers (Fig. 1).

It is well known that the occurrence of sand liquefaction phenomena may cause significant modifications of soil geotechnical properties and reduction of load-bearing capacity, with potential destruction and damages to structures and even human casualties. It is therefore crucial to improve the understanding of the factors that may induce liquefaction (Krinitzsky et al. 1988; Mitchell and Soga 2005; Chen et al. 2008). Some of these factors, such as earthquake magnitude, depth of the groundwater table, peak ground acceleration, and sediment grain size, are relatively well defined (Youd and Perkings 1978; Ishihara 1993; Kramer 1996; Bray and Sancio 2006; Chang et al. 2011) although simplified models of soils are used. However, little is known about other relevant geological parameters, in particular sedimentary facies and lateral facies changes, and changes in texture and composition of sediment in liquefiable layers. Recent papers have shown the potential of detailed sedimentological studies for the comprehension of liquefaction processes (Hurst et al. 2011; Owen and Moretti 2011; Ross et al. 2011, 2013; Quigley et al. 2013; Fontana et al. 2015; Rodriguez Pasqua et al. 2015; Amorosi et al. 2016; Cobain et al. 2017; Giona Bucci et al. 2017). The composition of sand dikes and blows represents an important tool to identify the liquefied source layers in the subsurface, while sedimentary structures and texture may provide information on pulse injection mechanisms of liquefied sands along fractures (Nichols et al. 1994; Hurst et al. 2011; Ross et al. 2014; Fontana et al. 2015).

Physical experiments in New Zealand and in the United States have shown that liquefaction can be induced and monitored with field-scale

Published Online: Month 2018
 1527-1404/18/088-000

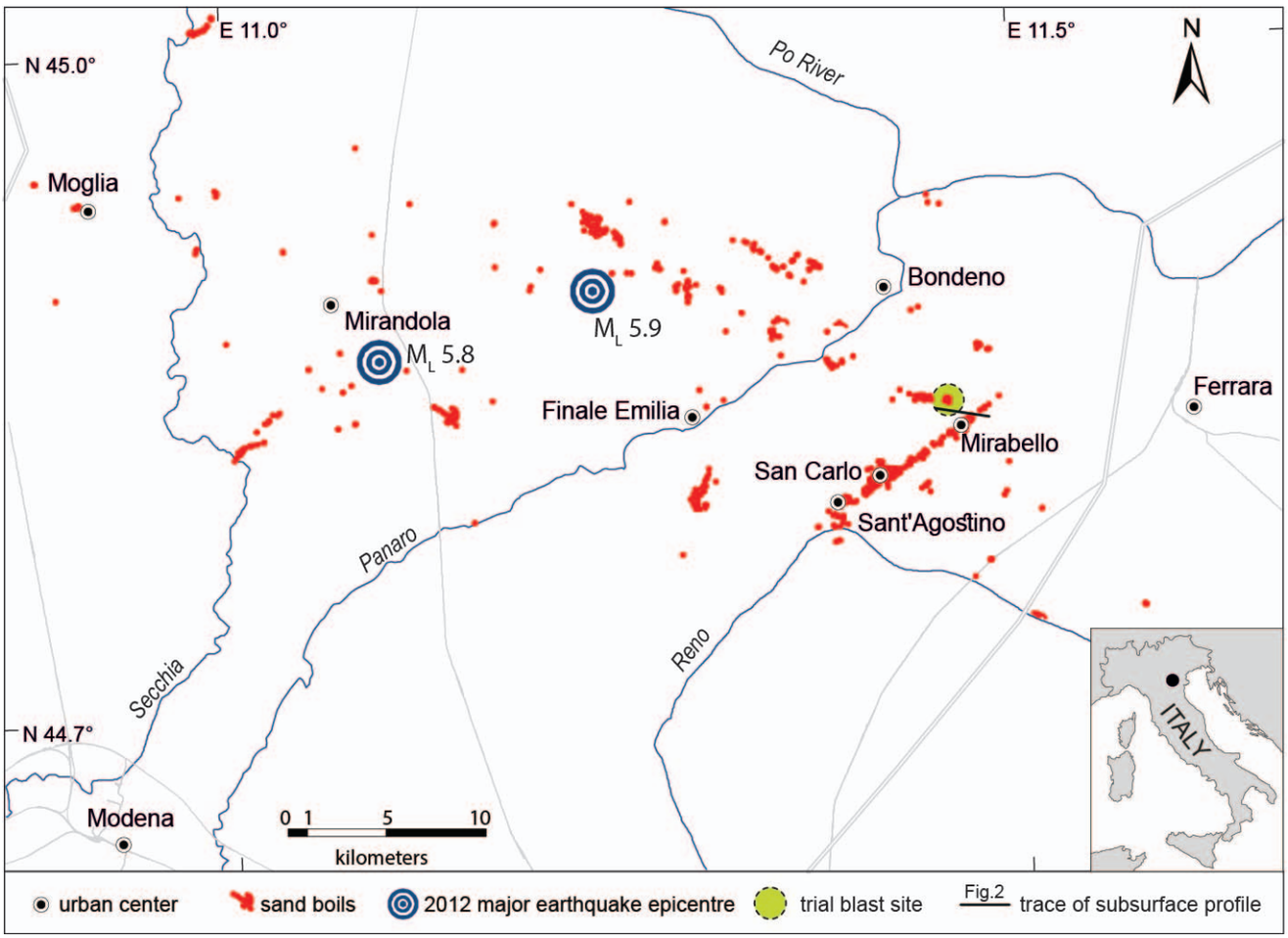

FIG. 1.—Map of the Emilia alluvial plain showing the blast test site of Mirabello. The area was affected by the 2012 earthquakes (two major epicenters are located) that generated numerous sand boils (red dots) (data from Emergeo Working Group 2013; Caputo and Papathanasiou 2012). At the end of 18th century the course of the Reno River was artificially forced to reach the Adriatic Sea. The studied site is located just northeast of the diversion point, along the buried paleochannel.

blast tests in order to study the associated effects on soil characteristics (Ashford et al. 2004; Rollins et al. 2004; Wentz et al. 2015; Finno et al. 2016). Following these experiments, in 2016 a research project on blast-induced liquefaction at the field scale was performed at a trial site located in Mirabello (Ferrara, Italy; Amoroso et al. 2017) (Fig. 1), a small town strongly affected by liquefaction phenomena during the 2012 Emilia earthquake (Caputo and Papathanasiou 2012; Emergeo Working Group 2013; Fioravante et al. 2013). The stratigraphical, geotechnical, and geophysical properties at the test site were investigated in detail, through several multidisciplinary techniques (Amoroso et al. 2017). Two cores (10 and 20 m deep) and two shallow trenches in the test site allowed reconstruction of the stratigraphy of sediments in the subsurface and the sampling of sands.

Here, the composition of sand blows ejected during the blast test, compared with the composition of different horizons of buried fluvial sediments as deep as 20 m, has proved to be an important tool to identify the liquefied layers. Moreover, for the first time the sands involved in the blast-test experiment are characterized by a relatively high fine-grained content compared with previous blast experiences performed in cleaner sands. This has allowed a better understanding of the selective processes undergone by sediments during the ejection.

GEOLOGICAL SETTING

The Po Plain represents the sedimentary filling of the Apennine foredeep, made up of a thick succession of Miocene–Quaternary marine and continental deposits. Beneath the alluvial plain, the fault–fold structures of the external portion of the Apenninic orogenic wedge are buried (Boccaletti et al. 2004; Ghielmi et al. 2013). Buried anticlines formed mainly during the Cenozoic in response to the collision between the European and the Adria plates (Ricci Lucchi 1986; Argnani et al. 2006). The ongoing deformation of the buried fault–fold structures, superimposed on a fast regional subsidence affecting mainly the southern portion of the foredeep basin (Carminati et al. 2005) allowed a thick accumulation of fluvial sediments, primarily due to the Po River and multiple Apenninic tributaries. The thickness of the sedimentary infill is highly variable, from 4 km in depocenter area, close to the Apenninic mountain front, to a few hundred meters in correspondence of the buried anticlines (Mariotti and Doglioni 2000; Ghielmi et al. 2013).

The thick Quaternary successions are punctuated by several unconformities controlled by the glacio-eustatic transgressive–regressive fluctuations (Amorosi et al. 2008; Garzanti et al. 2011), supporting the subdivision of the succession into allostratigraphic units. The sediments discussed in this research are ascribed to the last depositional cycle,

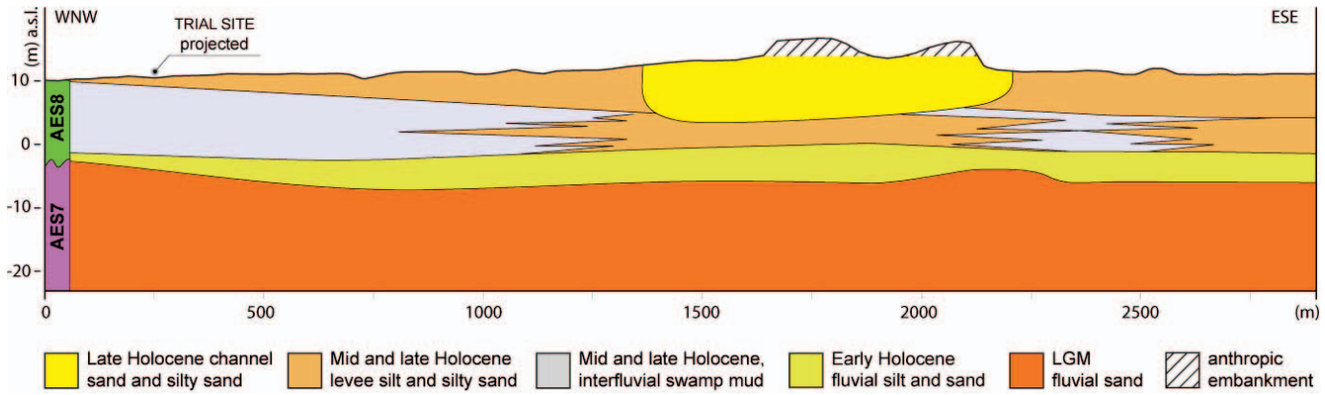

FIG. 2.—Simplified stratigraphic section of the Ferrara alluvial plain (modified from Geotema 2014). The deepest succession (AES7) is dominated by sands accumulated during the Last Glacial Maximum (LGM) (late Pleistocene). The overlying succession (AES8) is made up of Holocene fluvial channel and levee sands and silts alternating with silt and clay recording wide continental swamps. The upper portion of the AES8 is dominated by the large sand body of the Reno River flanked by its levee and interfluvial deposits

referable to the upper portion of the Villa Verrucchio Subsynthem (AES7) and the Ravenna Subsynthem (AES8) (Fig. 2). The two units, here consisting entirely of fluvial sediments, are separated by a regional discontinuity surface marked by widespread organic-rich and weakly developed paleosols (Stefani et al. 2018).

In the study area, the upper portion of the Villa Verrucchio Subsynthem (AES7) is dominated by sands accumulated during the Last Glacial Maximum (LGM). The Ravenna Subsynthem (AES8) is made up of silt, silty clay, organic-rich clay, and peats recording wide continental swamps intercalated with sands and silty sands deposited into fluvial channel and levee settings by various rivers. The upper portion of the AES8 is dominated by the large sand body of the Reno River, flanked by its levee and by interfluvial depression deposits (Stefani et al. 2018).

The region is affected by significant seismic activity due to the compressional deformation of fault–fold structures of the buried orogenic wedge. In May 2012, a severe seismic sequence induced significant human casualties, diffuse damage of buildings, and widespread liquefaction of fluvial sand and silt bodies, buried in the shallow subsurface (Caputo and Papathanasiou 2012; Emergeo Working Group 2013; Fioravante et al. 2013). The subject of this study, the southwestern part of the Ferrara Province, at San Carlo and Mirabello, was severely affected by liquefaction phenomena (Fig. 1).

MATERIALS AND METHODS

Blast Test.—The blast technique is based on a controlled detonation of explosives aimed at generating long-duration cyclic shaking of the ground and testing the *in situ* soil liquefaction potential, as recent experiments in New Zealand and the United States have shown (Wentz et al. 2015; Finno et al. 2016). A blast test produces accelerations whose frequencies are significantly higher than the real earthquakes, but the obtained ground velocity and displacement amplitudes are similar to those generated by a strong earthquake. Sequential blasts can also induce multiple shear strain cycles and generate a build-up of excess pore pressure, inducing liquefaction. *In situ* geotechnical monitoring, laboratory investigations, and geophysical surveys are usually coupled with the detonations to optimize their effectiveness (Gohl et al. 2009; Ashford et al. 2004; Rollins et al. 2004) and to evaluate variations in soil parameters before and after liquefaction. The first Italian blast experiment at the target site of Mirabello (Ferrara, Italy) was performed on May 2016 with various purposes, including the evaluation of the source layers of the blast-ejected sands and the interpretation of the blast-induced liquefaction mechanism. The controlled blasting experiment induced liquefaction in the trial field site because sand boils, mixes of sand and water that reach the surface and commonly form sand volcanoes (e.g., Marcuson 1978), were observed (Amoroso et al. 2017). The blast research activities (Fig. 3) included an intensive geological, geotechnical, and geophysical campaign before and after the implementation of two blast sequences. Pore-pressure transducers and settlement profilometers were installed in order to measure, during and after the blast test, the generation and subsequent dissipation of the pore-water pressure along with the vertical deformations. Based on the subsoil model and liquefaction assessment provided by Amoroso et al. (2017), the blast layout was designed considering two sequences of blast charges to detonate separately. Further details of the blast test are reported in Passeri et al. (2018) and Pesci et al. (2018).

Cone-Penetration Test.—Important stratigraphic information weas deduced from the comparative analysis of the cone-penetration tests (CPT) performed in the surroundings of the trial area (Fig. 3) for the seismic microzonation studies of Mirabello municipality (CPTuB11, CPTu019, CPTu13244; Geotema 2014) and for the blast-test experiment (CPTu1, CPTu2, CPTu3; Amoroso et al. 2017). The vertical variation trends of the penetration logs supported the recognition of various fluvial depositional bodies, paleosols, and peat levels.

Sampling.—A total of 35 samples were collected and analyzed for grain size and composition. Samples are representative of blast-induced liquefied sands and of sands in the subsurface (Tables 1, 2, Figs. 3, 4). Thirteen samples come from two cores (S1 and S3) located in the test site that allowed reconstruction of the stratigraphy and sand horizons from the surface down to 20 m (Fig. 4, Table 1). Sampling was particularly dense in the interval between 5 and 8 m, considered as the most critical liquefiable layer. Two samples come from the helical system that anchored the CPT truck at 2 m depth (ANC1, ANC2). Eight samples are liquefied sand induced by the blast test: three are representative of boils (C1, C2, C5) collected immediately after the first detonation within the 5 m-radius blast ring (Fig. 5A), and five were collected during and after the blast experiment around blast monitoring equipment (instrumented micropile and profilometers). Sample SB2012 is a sand boil from the 2012 Emilia earthquake in the studied area (Fig. 3A). Finally, eleven samples are from dikes that crosscut the shallow subsurface in 2 trenches (2.0–2.5 m deep) dug in the test site named BH15 trench (8 m long) and MPA4 trench (10 m

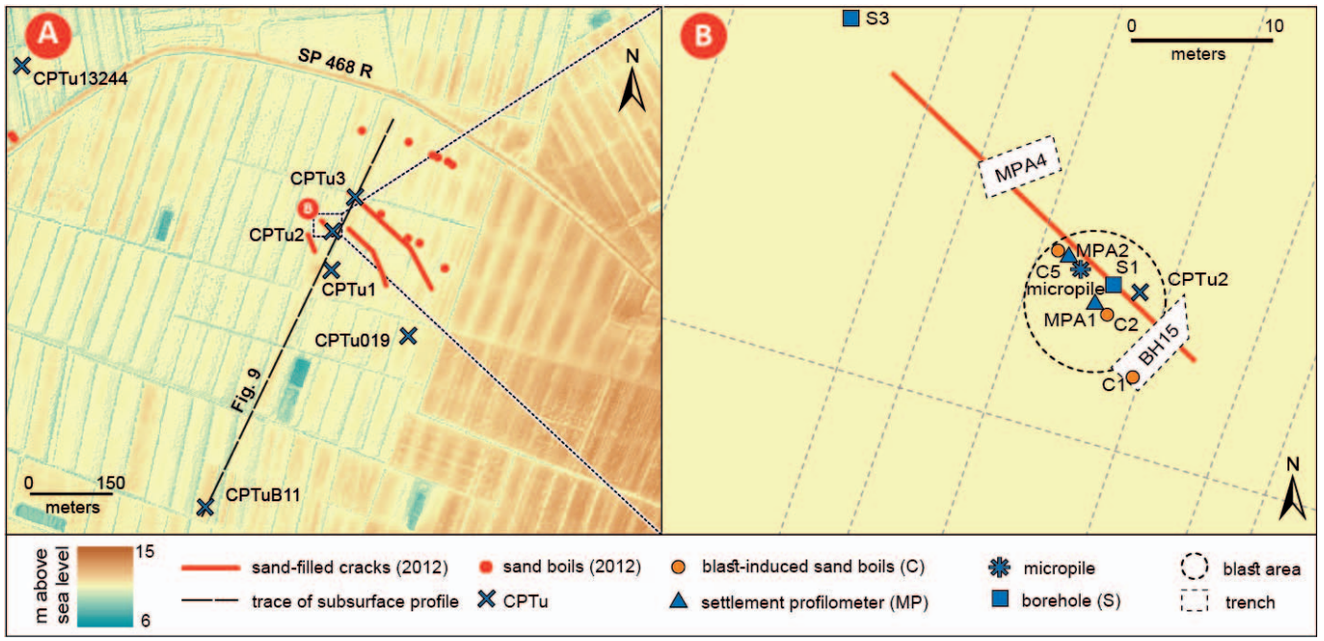

FIG. 3.—**A)** Location map of the trial Mirabello blast test site showing the CPTu tests and 2012 sand boils (modified from Amoroso et al. 2017). **B)** Detail of blast investigations with location of blast-induced sand boils and trenches.

long) (Fig. 3). Table 1 and Figure 5B and C report more detail on dike depth and shape. Samples are from the center of the dikes. Exploratory trenches were excavated by Istituto Nazionale di Geofisica e Vulcanologia (INGV, Rome, Italy) across the 2012 sand blows, approximately 5 to 12 m from the blast center. Dikes are not observed to reach the surface in the trench cross section. They likely represent sands liquefied during the 2012 earthquake and possibly previous events (INGV, work in progress).

Grain-Size Analyses.—32 samples were analyzed using standard techniques: mechanical sieving for the sandy fraction and hydrometer analysis for fine-grained sediments. Sand samples consisting of a few hundreds of grams were washed with dilute H_2O_2 to remove organic matter and were air dried and mechanically sieved for granulometric and compositional analyses. Grain-size analyses are reported as the granulometric curve in Figure 6. Table 1 reports the fines content (FC) which represents percentage of particles finer than 0.075 mm. D_{60}, D_{30}, and D_{10} are the diameters of the 60th, 30th, and 10th percentile of the granulometric curve. The coefficient of uniformity U is given by the ratio between D_{60} and D_{10}, and the coefficient of curvature C is function of D_{30}, $D_{60,}$ and D_{10}:

$$C = \frac{D_{30}^2}{D_{10} \cdot D_{60}} \quad (1)$$

According to the Unified Soil Classification System (USCS, ASTM D2487-11 2011) the sands characterized by $U > 6$ and $1 < C < 3$ are well-graded (or poorly sorted).

Compositional Analyses.—Modal analyses were carried out on 32 samples of sands and on the sandy fraction of sandy silt. Point counting under transmitted-light microscopy was performed on the 0.125–0.250 mm fraction, according to the Gazzi-Dickinson method designed to minimize the dependence of the analysis on the grain size (Zuffa 1985) and to support a comparison with previous compositional studies of the area (Lugli et al. 2004, 2007). Results of point counting (300 grains for each section) are presented in Table 2. For textural and provenance considerations we refer to studies of Weltje and Von Eynatten (2004), Arribas and Tortosa (2003), and Garzanti et al. (2011); detrital carbonate lithics were identified according to Fontana (1991). Components not related to the original sand composition, such as authigenic carbonate concretions, were excluded from the final calculations.

RESULTS

Stratigraphy of the Blast Test Site

The shallow sedimentary succession (0–20 m) involved in the blast test was deteiled by two boreholes integrated with CPTu data (Fig. 4) and interpreted within the knowledge framework deriving from a recent study on the geology of the area (Minarelli et al. 2016, and references therein). We recognize different units from older to younger:

- Unit A, from 20.5 m to 17 m below the surface. This is the deepest unit involved in the blast-test investigation, and is formed by gray, medium- to coarse-grained sands. From the integration of the blast-test data with evidence of regional geology, we can assume that the unit represents the upper portion of the AES7 subsynthem, and accumulated into a braided-river environment mainly during the Last Glacial Maximum (LGM).

Sediments above unit A represent the upper portion of AES8 and show a complex sedimentary architecture. They can be subdivided into three superposed units:

- Unit B1 (from 17 to 7.7 m). It consists of fine- to medium-grained sand intercalated with poorly sorted silty sand. The lower portion, between 16 and 17 m, is coarser grained. At 13 m a thin silty layer is present. Based on the detailed correlation of the CPTu and stratigraphic core logs, the interval can be interpreted as a meander channel body. An organic-rich layer within the unit in an adjacent area has been dated 4440 ± 40 yr BP by ^{14}C (Amorosi et al. 2008; Stefani et al. 2018).
- Unit B2 (from 7.7 to 5.9 m). It is formed by fine-grained sand and silty sand, with subordinated intercalations of silt and, in the lower portion,

TABLE 1.—*Granulometric properties of the analyzed samples: FC is the fines content; D_{60}, D_{30}, and D_{10} are the diameters of the 60th, 30th, and 10th percentiles of the granulometric curve; U is the coefficient of uniformity; C is the coefficient of curvature.*

Samples	Description	FC (%)	D_{60} (mm)	D_{30} (mm)	D_{10} (mm)	U	C
Anc 1	Anchor of CPTu2 piezocone test	80.75	0.0081	0.0014	-	-	-
Anc 2	Anchor of CPTu2 piezocone test	91.67	0.0047	-	-	-	-
S1 4.8	Borehole S1 4.8–4.9 m	71.52	0.0378	0.0040	-	-	-
S1 5.9	Borehole S1 5.9–6.1 m	77.81	0.0473	0.0161	0.0013	36.6	4.2
S1 6.2	Borehole S1 6.2–6.3 m	61.40	0.0724	0.0248	0.0021	34.6	4.1
S1 7.0	Borehole S1 7.0–7.3 m	41.62	0.1325	-	-	-	-
S1 7.3	Borehole S1 7.3–7.4 m	32.24	0.2008	-	-	-	-
S1 7.4	Borehole S1 7.4–7.5 m	39.99	0.1570	0.0447	0.0047	33.1	2.7
S1 7.7	Borehole S1 7.7–7.8 m	39.80	0.1552	0.0434	0.0046	33.4	2.6
S1 9.4	Borehole S1 9.4–9.5 m	28.52	0.2178	0.0843	0.0066	33.1	5.0
S1 14.0	Borehole S1 14.0–14.1 m	36.05	0.2141	0.0420	0.0040	53.2	2.0
S1 18.2	Borehole S1 18.2–18.3 m	28.12	0.2868	0.0890	0.0068	42.1	4.1
S3 5.5	Borehole S3 5.5–5.6 m	96.20	0.0206	0.0073	-	-	-
S3 6.5	Borehole S3 6.5–6.6 m	75.59	0.0388	0.0099	-	-	-
S3 8.5	Borehole S3 8.5–8.6 m	39.80	0.1921	0.0268	0.0021	93.4	1.8
S 1B NW	BH15 trench 0.2 m	10.15	0.2726	0.1574	0.0743	3.7	1.2
S 2 NW	BH15 trench 1.4 m	25.26	0.2059	0.1245	0.0047	43.4	15.8
S 4 SE	BH15 trench 0.2 m	14.37	0.2543	0.1534	0.0306	8.3	3.0
S 5 SE	BH15 trench 1.3 m	19.73	0.2489	0.1410	0.0339	7.3	2.4
S 6 SE	BH15 trench 0.5 m	15.29	0.2922	0.1636	0.0201	14.6	4.6
S 8 SE	MPA4 trench 0.3 m	23.62	0.2028	0.1027	0.0060	33.9	8.7
S 9 SE	MPA4 trench 0.6 m	21.40	0.2105	0.1169	0.0059	35.7	11.0
S 10 SE	MPA4 trench 1.6 m	24.71	0.1965	0.1011	0.0068	28.7	7.6
S 11 NW	MPA4 trench 2.2 m	19.76	0.3029	0.1557	0.0057	53.4	14.1
S 12 NW	MPA4 trench 2.0 m	22.22	0.3118	0.1493	0.0028	113.1	25.9
C1	Blast sand boil	7.13	0.3271	0.1998	0.1058	3.1	1.2
C2	Blast sand boil	6.89	0.3051	0.1870	0.1085	2.8	1.1
C5	Blast sand boil	11.70	0.3643	0.2294	0.0320	11.4	4.5
LP1	Micropile sand boil	4.61	0.3292	0.2066	0.1313	2.5	1.0
LP2	Micropile sand boil	22.54	0.1803	0.0963	0.0399	4.5	1.3
LPS	Micropile trench	10.70	0.2477	0.1560	0.0710	3.5	1.4
MPA1	MPA1 profilometer trench	11.43	0.3490	0.2097	0.0523	6.7	2.4
SB 2012	2012 Sand boil	7.30	0.250	0.175	0.095	1.4	0.7

argillaceous levels. The interval can be interpreted as a fluvial levee complex, laterally grading into crevasse splays probably accumulated between 4000 to 3000 years ago.

- Unit B3 (from 5.9 to 0 m). Interfluvial depression and distal levee deposits made up of: silt and clayey silt with subordinate coarser-grained sandy levels, interpretable as an interfluvial depression (5.9–4.4 m); sandy silt layer with diagenetic carbonate nodules interpretable as a paleosol (4.4–4.1 m) associated with an emersion phase (Roman surface); dark-colored plastic silt and clay (4.1–2.2 m) with an intercalation of organic-rich clay and peat (3.1–3.5 m) (1080 ± 30 yr BP by ^{14}C; Amoroso et al. 2017). Organic-rich levels are common also in the upper portion of the unit, recording widespread interfluvial depression marshes; silty clay and silt (2.2–0.7 m) referable to the distal portion of crevasses splays of the paleo–Reno River (post Medieval, up to the 18th century); reworked materials by agricultural practises (0.7–0.0 m), containing muddy sediments with brick fragments and extruded sands liquefied during the 2012 Emilia earthquake.

Grain-Size Distribution

The analyzed samples range from almost pure sands to silt with a variable content of sand and clay. Samples from cores (Fig. 6A) show a gradual increase in grain size from shallow to deepest samples. In particular, samples from the upper portion (up to 6.5 m) are the finest, made up of coarse silt and sandy silt with a clay content higher than 10%. Sands from 7 m to 18.5 m are coarser grained and fit in a narrow field predominantly made up of fine- and medium-grained sands; the amount of silt is 20 to 30%, and the percentage of clay is lower than 10%.

Induced liquefied sands are almost pure sands (Fig. 6B) with a very narrow range around medium-grained sand. The amount of silt and clay is less than 10% (except LP2: 18%).

The dike samples are similar to blast-liquefied sands, but with a slightly higher percentage of silt and clay (up to 24%); clay is less than 10%, except in sample S12NW (Fig. 6B). Samples are well sorted. We did not observe significant grain-size variation along dikes at different depths (0.2 to 2.2 m; Table 1).

The fines content (FC, Table 1) in cores ranges between 32 and 78% in samples from 5.9 to 7.7 m and is lower (28–39%) in deeper samples. A distinctly lower FC content (< 25%) is recorded in the blast-induced liquefied sands (FC 5–22%) and in trench samples (FC 10–25%). The coefficients of uniformity U and curvature C in samples from the boreholes show that the silty sands are well-graded (i.e., they contain particles with a wide range of sizes). In contrast, the blast-liquefied sands and dikes are well sorted.

Composition of Sands

Data from modal analyses are reported in Table 2 and in the ternary diagram Q + F (quartz + feldspars), L (siliciclastic fine-grained lithics), C

TABLE 2.—*Compositional modal analyses of examined sands (r.f., rock fragment). Composition is determined based on transmitted-light spectroscopy of the 125–250 μm fraction.*

SAMPLES	ANC 1	ANC 2	S1 4.8	S1 5.9	S1 6.2	S1 7.0	S1 7.4	S1 7.7	S1 9.4	S1 14.0	S1 18.2	S3 6.5	S3 8.5	S1A NW	S1B NW	S2 NW	S11 NW
Q																	
Quartz (single crystal)	25.3	29.0	41.3	32.0	43.3	38.7	27.7	39.3	33.0	26.0	41.3	32.7	37.0	33.3	38.0	34.0	35.3
Quartz (coarse-grained polycrystalline)	8.0	12.3	4.7	5.7	2.0	6.0	14.0	5.0	9.7	10.0	9.3	7.0	12.0	7.0	3.3	5.0	6.0
Quartz (fine-grained polycrystalline)	-	2.0	1.0	0.3	-	-	2.0	-	4.0	5.7	3.7	1.0	2.0	-	-	0.3	-
Quartz in plutonic/gneissic rock fragment	3.3	1.7	1.3	-	-	1.7	2.3	1.0	4.7	2.3	1.3	-	3.7	23	1.0	1.3	2.3
F																	
K-feldspar (single crystal)	8.3	5.7	10.0	6.7	3.0	5.3	5.3	13.0	6.7	9.7	3.7	1.7	6.3	9.0	9.3	6.7	9.3
K-fedspar in plutonic/ gneissic r.f.	-	-	-	-	-	-	0.3	-	-	0.3	0.3	-	-	-	-	-	0.3
Plagioclase	7.3	7.0	2.7	3.7	3.3	6.7	11.7	5.3	12.3	20.3	12.3	5.3	8.7	8.3	10.7	8.3	6.3
Plagioclase in plutonic/ gneissic r.f.	1.0	0.3	-	-	-	0.3	-	-	0.7	0.3	-	-	-	0.3	-	2.0	-
L																	
Low-grade metamorphic r.f.	9.3	9.3	9.0	4.7	8.0	9.0	5.3	2.7	5.0	3.3	2.3	13.7	3.3	4.0	3.3	7.3	9.3
Volcanic r.f.	0.3	1.3	1.0	0.3	-	-	-	-	0.3	-	0.7	2.0	3.0	0.7	0.3	2.0	3.7
Serpentinite	0.7	-	-	-	-	-	1.0	-	-	1.0	-	-	-	-	-	-	-
Shale	12.7	7.7	13.7	16.0	13.7	8.0	6.7	9.0	3.0	4.7	2.7	3.7	4.3	10.0	8.0	11.3	6.3
Siltstone	1.3	0.7	3.3	3.0	1.0	2.0	0.7	4.0	-	0.3	2.3	-	1.0	2.7	1.0	1.0	1.3
Micas and chlorites	6.0	1.7	3.7	13.7	11.3	3.0	7.3	3.7	4.7	4.0	2.7	19.3	4.0	2.7	3.0	2.3	2.7
Micas and chlorites in r.f.	-	0.3	-	-	-	0.3	-	-	0.3	0.3	1.3	2.0	-	-	0.3	0.7	0.3
Heavy mineral	0.7	1.3	1.3	1.0	0.7	2.0	0.3	0.7	0.7	1.0	1.0	0.3	-	2.3	1.3	1.7	2.0
C																	
Calcite (single spar)	8.3	9.0	6.0	6.7	9.3	8.3	6.7	12.7	6.7	6.3	9.0	6.7	6.7	9.3	14.7	9.3	9.3
Sparitic limestone	2.7	1.7	-	1.7	-	2.0	3.3	1.7	2.7	1.0	1.3	0.3	5.7	5.7	1.3	3.3	3.3
Micritic limestone	2.7	2.0	0.3	2.7	2.3	4.0	4.7	1.3	4.7	2.7	4.3	2.0	0.7	1.3	2.7	1.7	1.3
Bioclast (clastic)	-	1.7	-	-	-	-	0.3	-	-	-	-	-	-	-	0.7	0.3	-
Glauconitic grain	0.3	-	-	-	-	-	-	-	-	-	-	-	-	-	-	-	-
Carbonate concretion (diagenetic)	0.3	0.3	-	1.7	1.3	2.0	-	0.3	0.3	-	-	1.3	1.0	1.0	-	0.3	0.3
Iron oxides	1.3	4.3	-	-	-	-	-	-	-	-	-	0.3	-	-	-	1.0	-
Undetermined grain	-	0.7	0.7	0.3	0.7	0.7	0.3	0.3	0.7	0.7	0.3	0.7	0.7	-	1.0	-	0.3
	100.0	100.0	100.0	100.0	100.0	100.0	100.0	100.0	100.0	100.0	100.0	100.0	100.0	100.0	100.0	100.0	100.0

(carbonate lithics) of Figure 7. This diagram, better than the traditional QFL, allows the compositional fields of fluvial sands in the Po plain to be differentiated as discussed by Lugli et al. (2007).

Fluvial Sands from Boreholes.—Fluvial sandy sediments in the subsurface (sands and the sandy fraction in sandy silt), both from cores S1 and S3, show varying compositions from lithoarenitic to quartz–feldspar-rich (Fig. 7A). They are made up of quartz (single crystal and polycrystalline) ranging from 36.6 to 55.6% of the bulk rock; the highest amounts are in the deepest sands at 18.2 m. Feldspars, both plagioclase and K-feldspar, vary from 6.3 to 30.6%. Siliciclastic lithics are fine-grained detrital rocks, siltstones and shales, and subordinate low-grade metamorphic rocks. Lithics range from 8 to 27.7% with minor amounts in deeper sands. Shales are well lithified, with an evident preferred orientation of clay minerals, and for these characters they appear to have a detrital origin, derived from older pelitic successions. Volcanites, spilites, and serpentinites are only minor components. Carbonate lithics range from 6.3 to 15.7% of the bulk sand and are made up of micritic and sparitic limestones; spars of calcite are also included, as they derive from the breakage of sparitic limestones and veins. Micas (muscovite and chlorite), glauconitic grains, and Fe-oxides are minor components. Few diagenetic concretions occur in some samples. Sands do not show any evidence of grain cementation, including the deepest ones.

In the Q + F, L, C diagram (Fig. 7A), sands in the subsurface show a well-defined trend from litharenitic to quartz–feldspar-rich compositions. In particular, sands at depth up to 7.7 m are, in different proportion, more litharenitic, rich in fine-grained sedimentary lithics (siltstones and shales) (Fig. 8A), while the deepest sands (samples from 8.5 to 18.5 m) are enriched in quartz and feldspars and fit in a well-defined field of arkosic composition (Fig. 8B, C).

Provenance of Fluvial Sands.—based on type and abundance of lithic grains, which are mainly sedimentary, both fine-grained siliciclastic and carbonate derived from the erosion of Apenninic sedimentary units, shallow sands up to 7.7 m indicate a clear Apenninic provenance referable to the paleo–Reno River. Deeper sands, richer in quartz and feldspars, with abundant micas and very low siltstones and shales, show affinities with the Po River sands. The deepest sample of sands at 18.2 m is the richest in quartz (Fig. 8C) and poorest in sedimentary lithics, and is linked to the older unit A, deposited by the Po River during the Last Glacial Maximum.

Blast-Induced Liquefied Sands.—Liquefied sands from sand boils (Figs. 7B, 8D) are quite homogeneous in composition. Total quartz ranges from 40.4 to 52.6%. Feldspars (both plagioclase and K-feldspar) vary from 7 to 15.4%. Fine-grained siliciclastic lithics, made up of siltstones, shales, and low-grade metamorphites, account for 15 to 25.8% of the whole sands.

TABLE 2.—*Extended.*

SAMPLES	S12 NW	S4 SE	S5 SE	S6 SE	S8 SE	S9 SE	S10 SE	C1	C2	C5	LP1	LP2	LPS	MPA1	MPA2
Q															
Quartz (single crystal)	35.7	37.1	37.3	40.3	34.0	42.7	29.7	25.7	30.7	40.0	32.7	37.9	32.0	31.7	36.7
Quartz (coarse-grained polycrystalline)	3.3	7.7	5.0	4.7	5.7	4.3	2.7	11.0	10.0	8.3	8.0	4.3	6.3	4.3	17.0
Quartz (fine-grained polycrystalline)	-	-	-	-	-	-	-	2.0	3.0	1.0	0.3	1.2	-	-	-
Quartz in plutonic/gneissic rock fragment	0.3	1.3	1.0	2.3	1.3	1.0	1.0	1.7	2.3	3.3	3.3	1.9	1.3	0.3	6.7
F															
K-feldspar (single crystal)	7.3	7.4	5.3	8.3	6.3	5.0	8.7	8.7	4.0	3.0	7.7	10.6	9.3	6.3	3.0
K-fedspar in plutonic/ gneissic r.f.	-	-	-	-	0.3	-	-	-	-	0.3	-	-	-	-	0.3
Plagioclase	8.0	7.4	8.3	4.7	9.0	5.7	10.7	6.7	4.0	3.7	8.0	4.0	6.7	6.7	5.0
Plagioclase in plutonic/ gneissic r.f.	-	-	-	-	0.3	-	0.3	-	-	-	-	-	0.3	-	-
L															
Low-grade metamorphic r.f.	9.0	6.8	3.7	5.3	8.0	7.3	13.7	10.3	14.7	4.0	9.7	9.6	9.7	16.3	5.0
Volcanic r.f.	3.0	2.6	1.3	1.7	0.3	-	0.7	0.7	0.7	2.7	-	0.9	-	1.3	-
Serpentinite	-	-	-	-	-	-	-	-	0.7	-	-	-	-	-	-
Shale	6.7	4.2	13.7	10.7	11.3	7.3	7.7	13.0	7.0	7.3	4.7	5.9	7.0	10.0	8.3
Siltstone	1.0	2.3	0.7	1.3	2.0	1.3	1.7	-	2.7	1.0	2.0	2.8	6.3	3.0	2.3
Micas and chlorites	3.3	3.9	5.3	5.0	3.7	4.0	4.0	4.0	4.0	4.3	3.7	3.7	2.0	4.3	3.0
Micas and chlorites in r.f.	-	0.3	-	-	0.3	-	-	1.0	-	0.7	0.3	-	-	-	0.3
Heavy mineral	0.3	2.2	-	-	1.0	1.3	-	1.0	0.7	1.3	3.0	0.6	2.3	1.0	-
C															
Calcite (single spar)	12.7	11.0	10.3	10.0	8.7	9.3	10.3	7.7	7.7	9.7	10.0	8.1	9.3	7.3	7.0
Sparitic limestone	3.3	2.9	2.7	4.0	3.3	4.7	4.7	3.3	2.7	4.7	4.3	3.4	3.7	4.7	0.7
Micritic limestone	3.3	1.9	2.3	-	2.3	2.3	2.7	-	3.3	2.0	0.7	2.2	1.3	1.3	2.7
Bioclast (clastic)	-	-	0.3	-	-	-	-	0.3	1.0	0.3	-	0.3	0.7	-	0.3
Glauconitic grain	-	-	-	-	-	-	-	-	-	-	-	-	-	-	-
Carbonate concretion (diagenetic)	1.0	-	1.7	0.7	0.7	1.7	1.0	2.0	0.7	1.3	1.0	1.6	1.3	1.3	1.7
Iron oxides	-	0.6	-	-	0.7	1.0	0.3	-	-	-	-	-	-	-	-
Undetermined grain	1.7	0.4	1.0	1.0	0.7	1.0	0.3	1.0	0.3	1.0	0.7	0.9	0.3	-	-
	100.0	100.0	100.0	100.0	100.0	100.0	100.0	100.0	100.0	100.0	100.0	100.0	100.0	100.0	100.0

Carbonate lithics, such as micritic and sparitic limestones, vary from 11.3 to 16.7%. Sands from micropile (see Table 1) show similar compositions with more variations in quartz content.

Composition of liquefied sands overlap that of the shallow fluvial sands down to the depth of 7.7 m and clearly differ from layers deeper than 8 m, higher in quartz–feldspar content.

Sand from Dikes in Trenches.—The sands filling the dikes in the trenches (Fig. 7C) show relatively homogeneous compositions. Total quartz ranges from 33.4 to 48%, and feldspars from 10.7 to 20%. Siliciclastic lithics, largely low-grade metamorphics and shales, range from 12.6 to 23.8%. Carbonate lithics vary from 13.9 to 19.4%. We did not observe significant variations in sands from single dikes at different depths. In the Q + F, L, C diagram, sands from dikes plot in the same field as shallow sands (up to 7.7 m).

DISCUSSION

The earthquake-simulation field experiment (blast test) carried out in Quaternary fluvial sediments of the Emilia plain induced subsurface liquefaction and the formation of sand blows. The grain size and composition of ejected sediments were compared with subsurface data from boreholes and trenches. The main findings of the study are discussed with a focus on the recognition of the source layer and grain-size segregation mechanisms during liquefaction.

Stratigraphic Framework

Data from two boreholes and several cone-penetration tests supported the reconstruction of a detailed stratigraphic framework of fluvial sediments in which the liquefiable layers are located (Fig. 9). The deepest portion of the section (unit A) consists of Po River sands deposited in the late Pleistocene into braided channels during Last Glacial Maximum and late Glacial times (LGM in Fig. 9). A thick sand body, interpreted as Po River channel fill (unit B1) is identified between 8 and 17 m. This is overlain by silty sands and silts from a paleo–Reno River levee body (unit B2, 5.9–7.7 m), which accumulated between approximately 4000 to 3000 years ago. The uppermost portion of the studied successions is largely formed by argillaceous sediments, deposited in interfluvial swamp and distal levee areas of the paleo–Reno River in Medieval and modern times (unit B3).

Source Layer Identification

The composition of sands liquefied by the blast test poses an important constraint in the recognition of the source layer. Measurements of excess

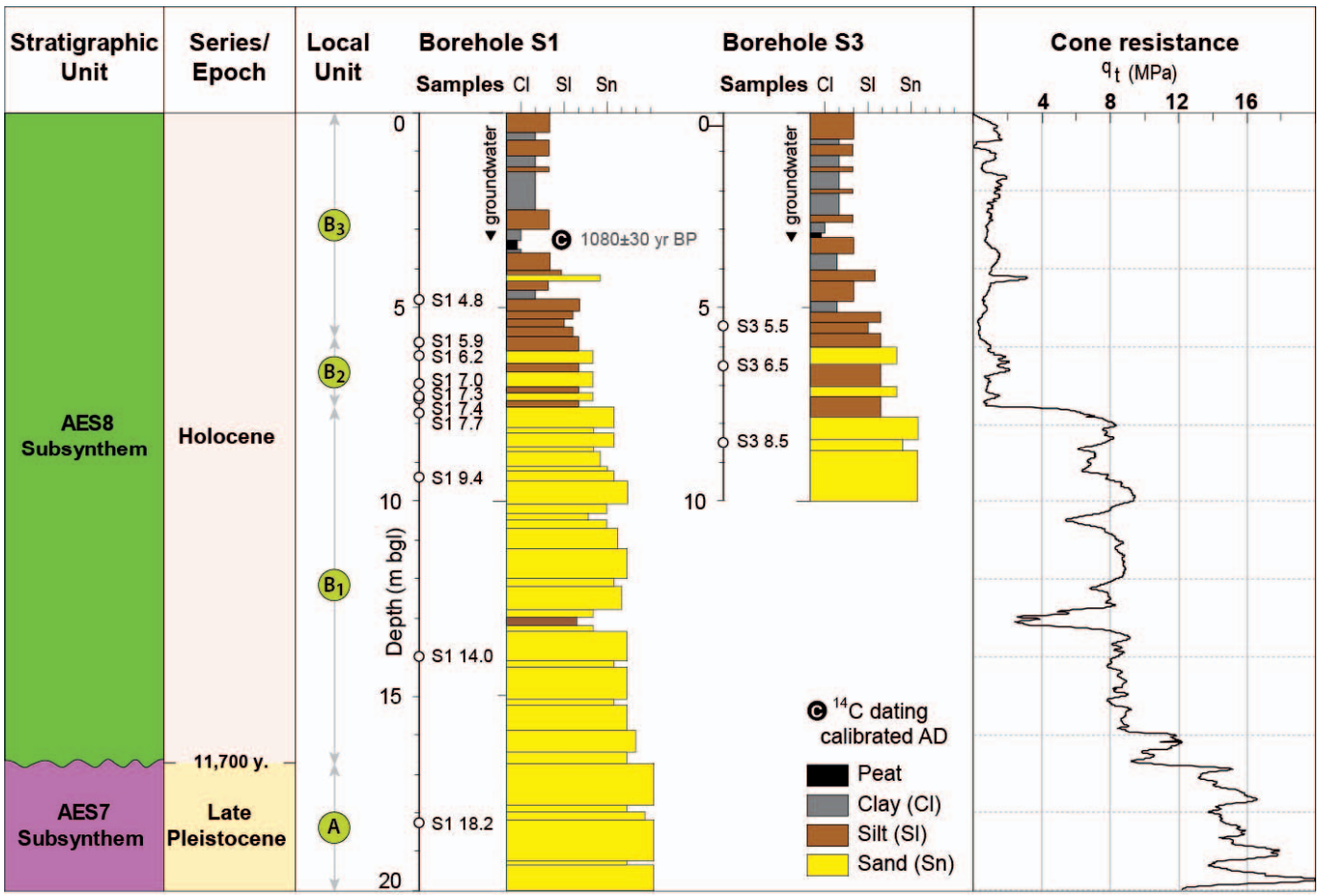

FIG. 4.—Stratigraphy of the two cores S1 and S2 coupled with cone-tip resistance profile. Four units are distinguished: A, B1, B2, and B3. Samples examined in this work are reported along the sections.

pore pressures and soil deformation during the blast monitoring have detected a wide liquefiable layer that extended at least from 6 to 12 m depth (Amoroso et al. 2017). However, only silty sands of unit B2, between 5.9 and 7.7 m deep, were ejected to the surface to form sand boils, as clearly deduced by petrographic analysis (Fig. 7). In fact, the composition of sands from blows shows close similarity with shallow sands of unit B2 at a depth from 5.9 to 7.7 m, while it clearly differs from deeper sands, which are richer in quartz and feldspar and poorer in sedimentary lithic fragments. These data indicate that the ejected layer largely corresponds to the fluvial Apenninic deposits of the paleo–Reno River, while the underlying sands referable to a paleochannel of the Po River (unit B1 and A) were not involved.

Our data also show that the composition of blast-induced sand boils overlap that of dikes in trenches of the blast area. As already reported by Amoroso et al. (2017), dikes are fractures infilled by sands injected upward during the 2012 earthquake or older events. This indicates that sand layers liquefied by seismic events are the same as induced by the blast test.

Results from the blast test fit well with data obtained from the study of the sands ejected in the nearby area of San Carlo during the M_L 5.9 earthquake (Fontana et al. 2015). Even in this case, sand composition and fabric indicate that liquefaction processes mainly affected sand layers at relatively shallow depth (6.8–7.5 m) characterized by litharenitic composition, and did not affect deeper sands, Holocene to Pleistocene in age, with a quartz–feldspar-rich composition.

In all these cases, the liquefied sands share a litharenitic composition, with abundant lithic fragments of micritic limestones, shales, and siltstones, usually rounded in shape, rather than sands rich in quartz and feldspars angular in shape. It is reported in the literature that the presence of rounded grains is one factor that can increase the liquefaction susceptibility (Kramer 1996), but very little data are available on petrography of liquefied sands and injectites (Ross et al. 2014). It could be that specific compositions favor liquefaction rather than others, but further studies are necessary to validate this factor.

Grain-Size Characteristics and Liquefaction Susceptibility

The grain-size characteristics of the examined sands are compared to data reported in the literature for sands ejected during earthquakes. Several

FIG. 5.—**A)** Blast-induced sand boils (C1) after the first detonation. Sample C1 is 15 cm distant from the center; the sand sheet is 7 cm thick. **B)** Sketch of sand dikes in the BH15 trench and location of sample S2 NW (1.4 m of depth from the topographic surface). **C)** Detail of sand dikes (see sample S2 for comparison). The width of dikes is around 5 cm

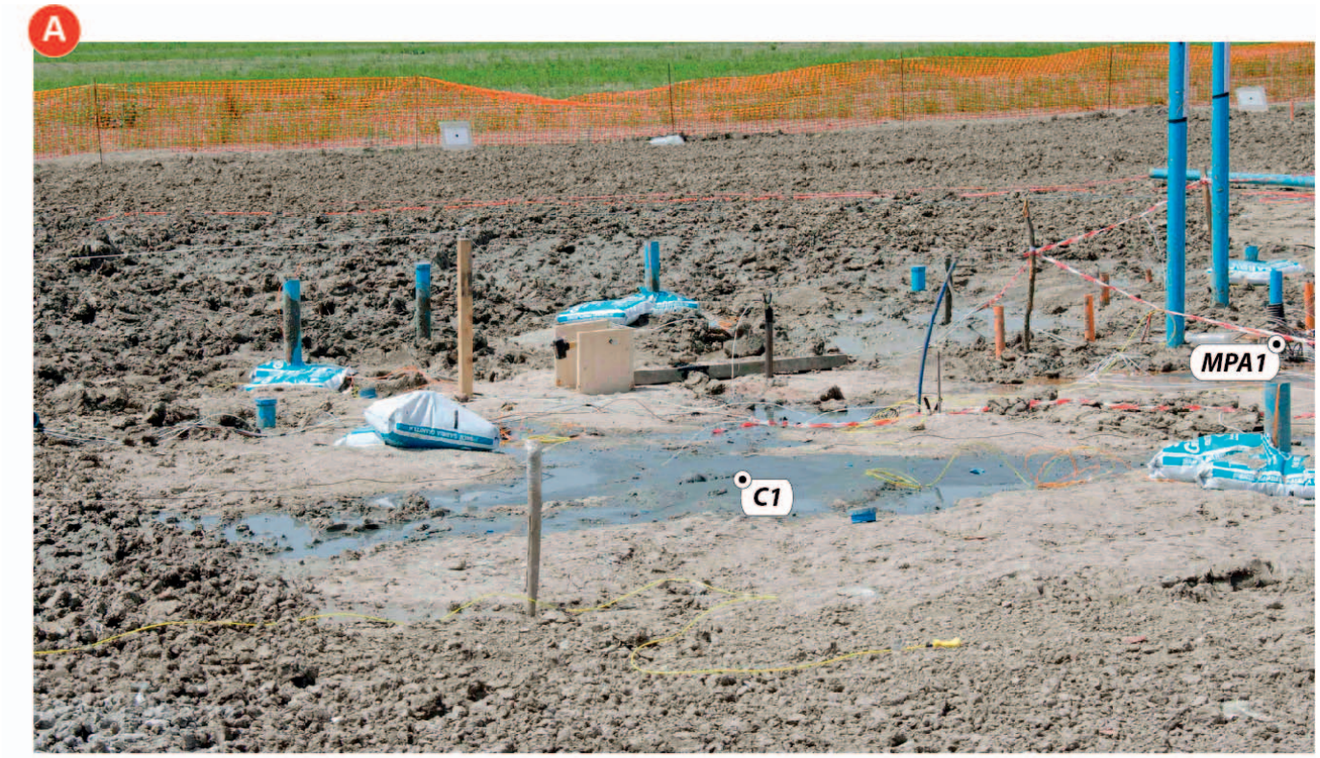
A
MPA1
C1

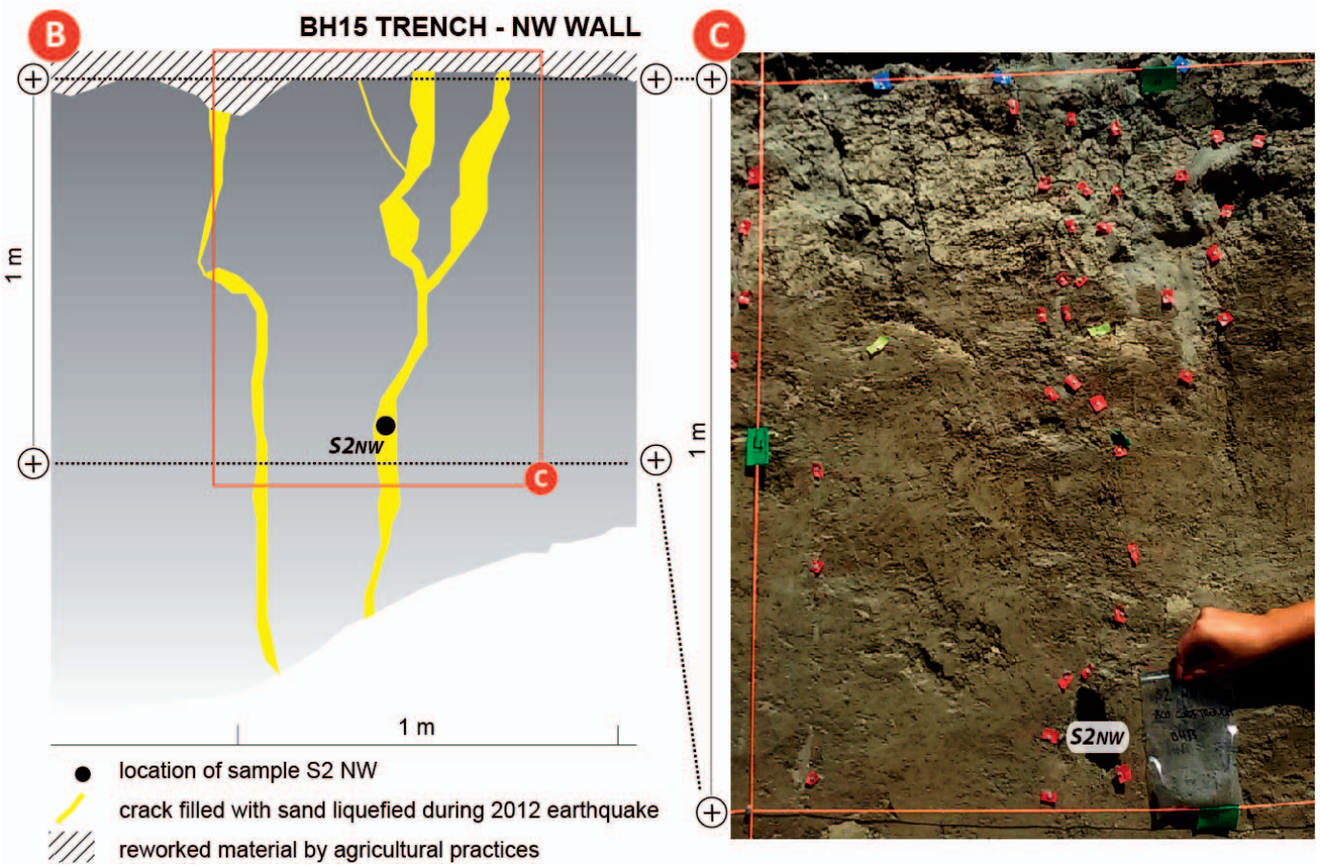
B
BH15 TRENCH - NW WALL
C
1 m
S2NW
C
1 m
1 m
S2NW
location of sample S2 NW
crack filled with sand liquefied during 2012 earthquake
reworked material by agricultural practices

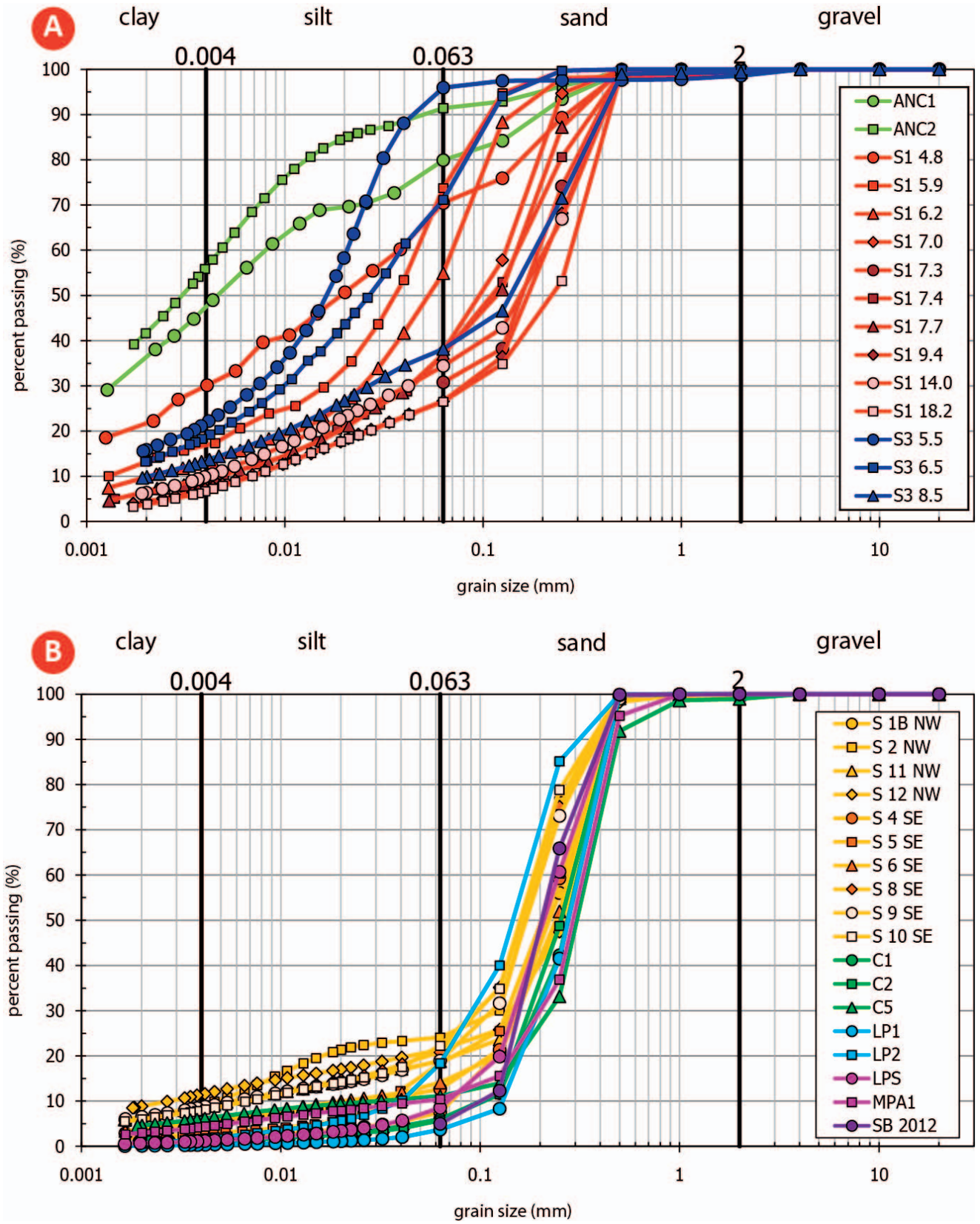

FIG 6.—Cumulative grain-size distributions of examined samples. **A)** Curves of samples from cores S1 and S2 plus anchor of CPTu2 piezocone test. **B)** Granulometric curves of induced liquefied sands (C1, C2, C3, LP1, LP2, LPS, and MPA1), of the SB2012 sand boil and of dikes.

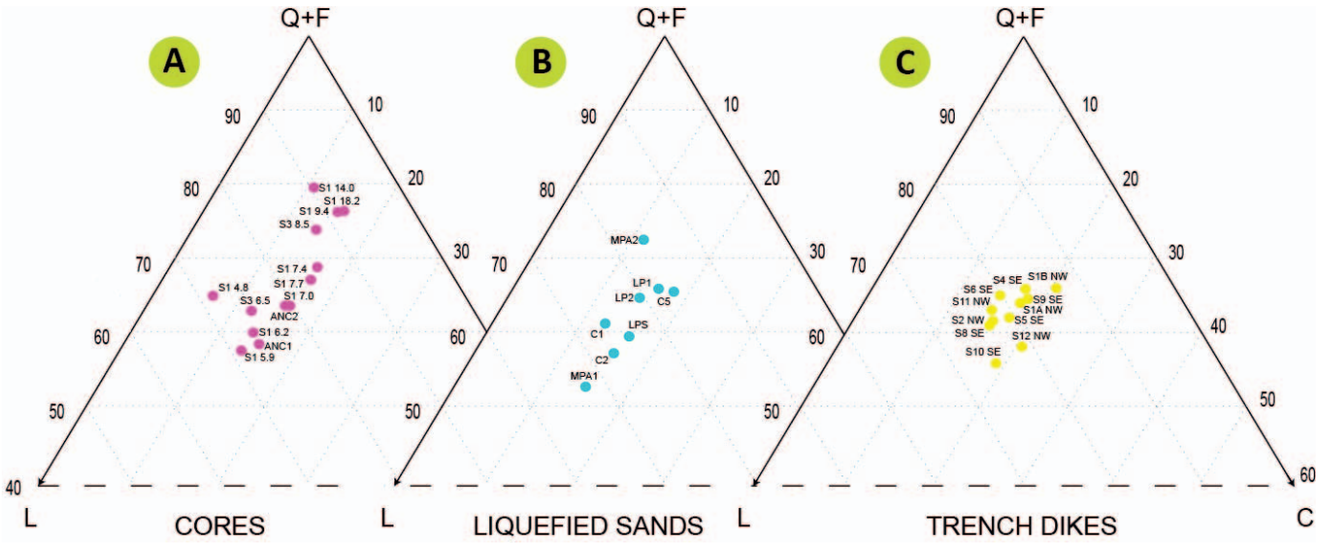

FIG. 7.—Q + F, L, C diagram showing the composition of examined sands. **A)** Sands from cores. **B)** liquefied sands from the blast test. **C)** Sands from dikes in trenches. Q, total quartz; F, total feldspars; L, siliciclastic lithic fragments; C, carbonate lithic fragments. Numbers in core samples refer to depth.

papers (Kishida 1970; Tokimatsu and Yoshimi 1983; Figueroa et al. 1995) report that mainly clean sand with a low natural clay content are susceptible to liquefaction, and report a cut-off for liquefaction susceptibility at a clay content of about 10–15%. The liquefaction susceptibility of fine-grained sediments has been debated over the last 20 years (e.g., Andrew and Martin 2000; Idriss and Boulanger 2008; Bray et al. 2014; Boncio et al. 2018): fine-grained sediments were considered incapable of generating the high pore pressures commonly associated with liquefaction (Kramer 1996). Only a few papers (Ishihara 1984; Chang et al. 2011) observed liquefaction of non-plastic silts, indicating that plasticity characteristics rather than grain size alone influence the liquefaction susceptibility of fine-grained soils. Non-plastic and cohesionless coarse silts with bulky particle shape are fully susceptible to liquefaction, while finer silts with flaky or plate-like particles generally exhibit sufficient cohesion to inhibit liquefaction (Ishihara 1993).

Since our study takes into consideration not only the characteristics of the sands that reach the surface but also those of the buried source layer, the effects of particle size in the liquefaction processes can be better outlined. Liquefied sands that reached the surface are well-sorted medium-grained sands with silt and clay content less than 10%; they fall within the expected parameters for liquefaction. However, when comparing liquefied sands with their source layer at 5.9–7.7 m depth (Fig. 6), we observe that "source" sands have a higher amount of fine-grained particles (silt and clay $> 30\%$; clay $< 15\%$). This has two interesting implications.

Firstly, the source beds can contain higher amounts of silt than reported in many previous liquefaction studies, indicating that also coarse silts and silty sands are fully susceptible to liquefaction. This aspect has to be considered while estimating the liquefaction potential hazard. Poorly sorted sands and finer-grained sediments are more susceptible to liquefaction phenomena than previously thought.

Secondly, we observe that there is a selective loss of fines in the dikes and sand volcanoes relative to the source beds, indicating that the liquefaction process appears to be able to select the diameters of the grains that reach the ground surface. This effect is well observed in the blast-induced liquefaction and in 2012 sand boil ejected in the same area (sample SB 2012, Fig. 6B) and to a lesser extent in the trench dikes (yellow curves in Fig. 6B).

Grain-Size Segregation during Liquefaction

Studies and experiments on liquefaction and fluidization of silty sand sediments, as occurs in dikes and sand volcanoes, suggest that sorting may occur within the source bed and dikes, and further separation occurs as the material is extruded (e.g., Diggs 2007; Ross et al. 2011). As pore pressure builds, finer-grained material may be moved into the surrounding sediment, forming an infiltration horizon and the slightly cleaner sediment can then break through this infiltration horizon and be injected upwards (Ross et al. 2011). Segregation can also occur in the injected dikes, with Ross et al. (2011) showing that fines can line the pipe walls as water flows radially out of the pipe due to the flow velocity gradient between the pipe and the ambient velocity in the surrounding sediment. This pipe-lining phenomenon has been observed elsewhere (Mount 1993; Diggs 2007; Kazerouni et al. 2011; Ross et al. 2014). Once the fluidized flow hits the surface then further segregation can occur. Ross et al. (2013) show for subaqueous sand volcanoes that clay and grain size decrease with increasing distance from the vent, which they interpret as a result of settling of the coarsest particles close to the vent, and preferential transport of the clay within the currents. Such processes also occur in subaerial systems: Quigley et al. (2013) show silt drapes on the top of sand volcanoes between liquefaction-inducing earthquakes, which they interpret as drapes from suspended sediment as ejected ground-water drained following the liquefaction event. The clay, and potentially some of the finer silts, become part of a pseudofluid (Di Felice 2010; Ross et al. 2014) and travels with the fluid phase whilst the larger particles are deposited from this suspension. Such fine-rich fluids can be seen in videos of earthquake-induced eruptions of sand volcanoes, such as those in Christchurch, New Zealand, described by Quigley et al. (2013). Pulse flows are hypothesized in dikes and sand blows in liquefaction sites due to the 2012 Emilia earthquake described by Fontana et al. (2015) and Rodríguez-Pascua et al. (2015). The sedimentary features (inverse and normal grading, vertical and concave lamination) suggest that fractures were rhythmically injected and filled by a slurry of sand and mud during the compression pulses, and emptied by the rushing of the slurry back down deep into the fractures during the extension peak, forming laminated structures in sand volcanoes on the top of the fractures

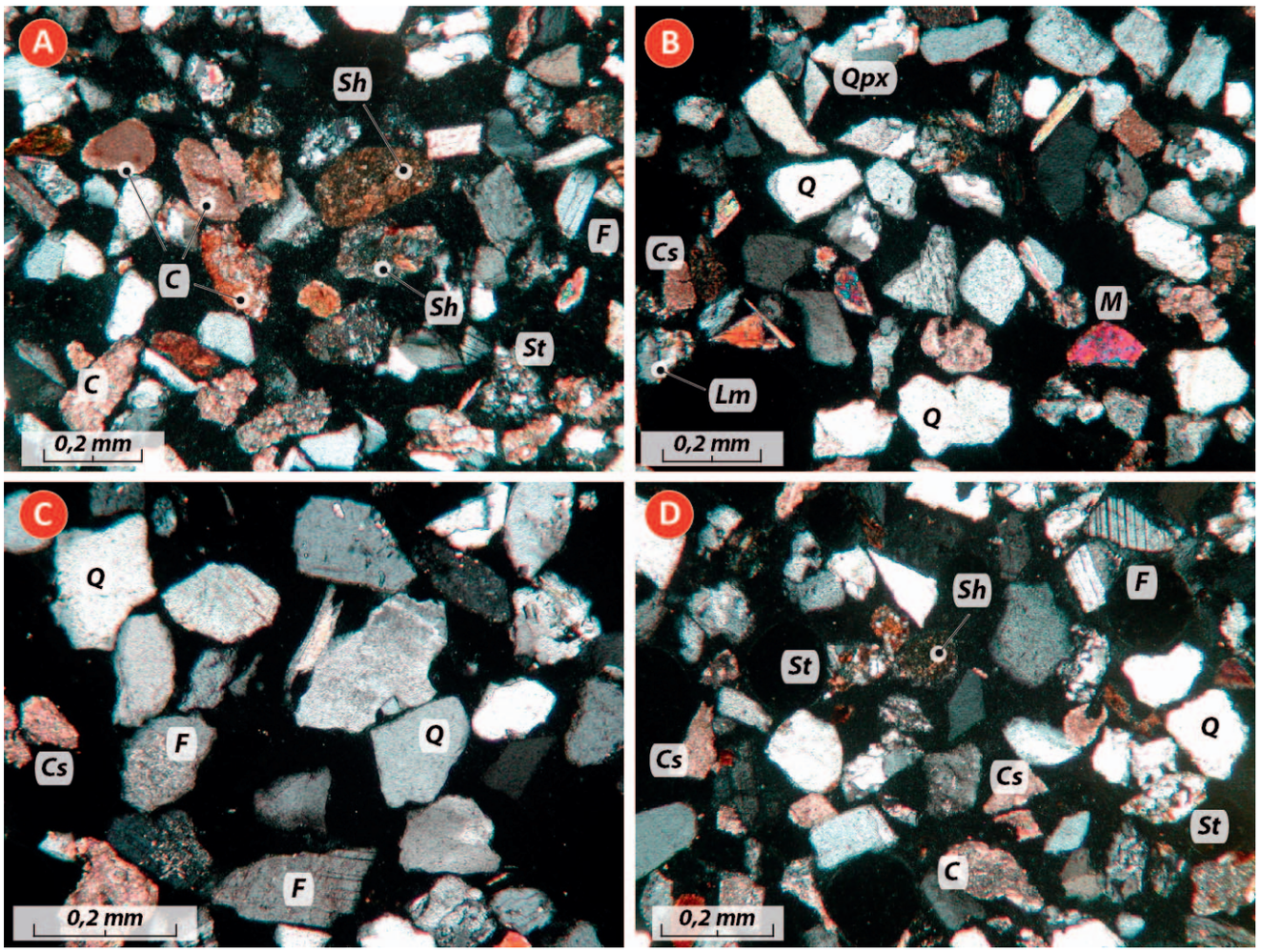

FIG. 8.—Photomicrographs of the examined sands. **A)** Sand from core S1 at depth of 6.2 m, with abundant sedimentary lithic fragments indicating an Apenninic provenance (Reno River). **B)** Sand from core S1 at depth of 9.4 m rich in quartz and feldspars referable to the paleo–Po River. **C)** Sands from the deepest horizon (S1 18.2) referable to the older Po River sands accumulated during the Last Glacial Maximum. **D)** Liquefied sands from sand boil C5. Transmitted light, crossed polars. Q, quartz; Qpx, polycrystalline quartz; F, feldspar; Sh, shale; St, siltstone; C, limestone; Cs, calcite spar, M, micas.

(millimeter- to centimeter-thick alternating graded laminae of sand and mud).

In interpreting results from our study (Fig. 10), we cannot exclude differences between shaking generated by the blast test versus earthquake. In fact, a blast test produces accelerations whose frequencies are significantly higher than real earthquakes, but the obtained ground velocity and displacement amplitudes should be similar to those generated by a strong earthquake (Amoroso et al. 2017). Data from this study confirm that some sorting occurs within dikes, and further sorting occurs as the material is extruded (both in blast-liquefied sands and in the 2012 earthquake sand boil), probably following the generated excess pore-water pressure. This may have caused the segregation and dispersion of the fine silt–clay content, producing highly sorted sand boils. Instead it seems that the selective mechanism due to ejection of liquefied sands has not influenced the sand composition (see also Fontana et al. 2015), and that disintegration or erosion of the most erodible grains due to the abrasive flow of sand grains is almost negligible.

CONCLUSIONS

- Study of the sands ejected during the blast test in the Mirabello area (Po plain), and comparison of their texture and composition with those of buried fluvial sediments as deep as 20 m supported a reliable source-layers identification.
- Ejected sands show a litharenitic composition that largely overlap that of the shallow Apenninic sands down to the depth of 5.9–7.7 m. These sands clearly differ from deeper sands, enriched in quartz and feldspars, largely referred to paleochannels of the Po River.
- Similarly the sands from the dikes show a composition compatible with that of the shallow sands of Apenninic affinity, suggesting that the liquefied layer during the 2012 seismic crisis is the same as that induced by blast test.
- The study indicates that silty sands and silts characterized by relatively high fines content (FC 32–76%) can also liquefy, differently from what reported in most of the literature.
- The liquefaction process appears to be able to select the diameters of the grains which reach the ground surface. Some sorting occurs within

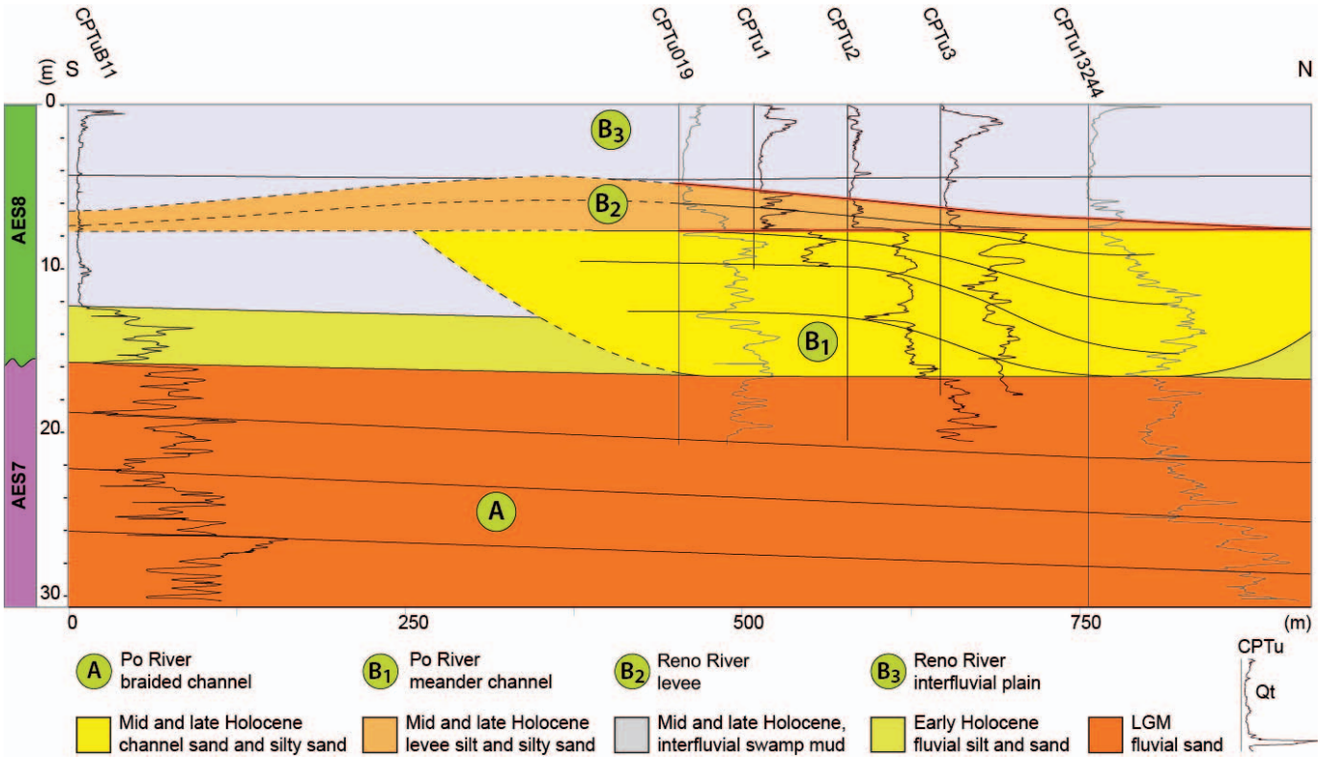

FIG. 9.—Stratigraphic scheme of the successions involved in the blast test. Source layer for the ejected liquefied sands is the unit B2 at 5.7–7.7 m depth, represented by levee silty sands and silts of the paleo–Reno River. Underlying sands of unit B1 were not involved in the ejection.

injected dikes, probably due to pulse flows, and further segregation occurs as the material is extruded following the generated excess pore-water pressure. This may have caused the dispersion of the fine silt–clay content, producing highly sorted sand boils.

- The study indicates that we have a significant tool for a better understanding of earthquake-induced liquefaction mechanisms, using textural and petrographic parameters to correlate ejected sands with their buried source beds. This is pivotal for the recognition of potential areas prone to hazardous sand liquefaction phenomena.

ACKNOWLEDGMENTS

The study was mainly funded by FIRB-Abruzzo project (http://progettoabruzzo.rm.ingv.it/it). Special thanks to Prof. Kyle M. Rollins for contributing to the realization of the blast-test experiment in terms of personnel and technical equipment. We are indebted to David Hodgson, Jeff Peakall, and Geraint Owen for the accurate revision and relevant suggestions that greatly improved the manuscript. Many thanks to Simona Marchetti Dori for the support in grain-size analyses and to Paolo Marco De Martini, Francesca Cinti, Alessandra Smedile,

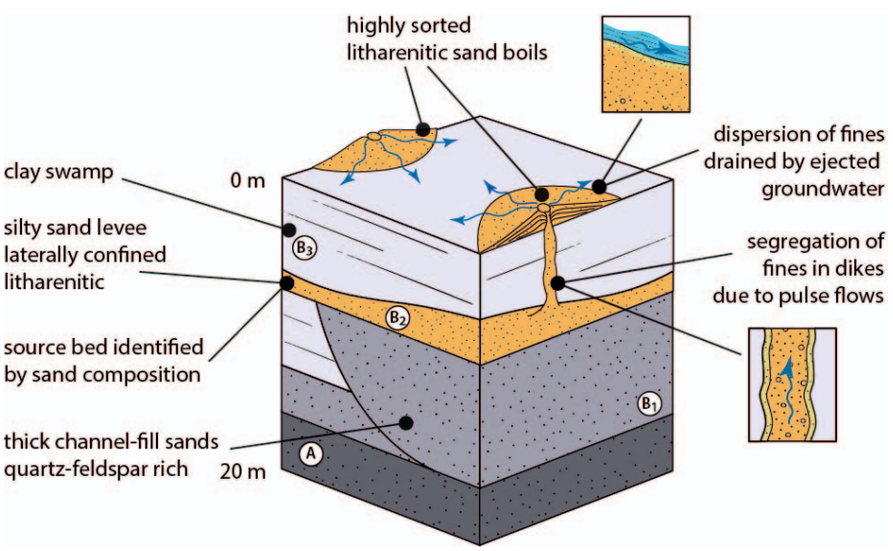

FIG. 10.—Sketch of the stratigraphy and various potential source layers in fluvial sediments of the Emilia alluvial plain, with compositional and grain-size characteristics. Selective mechanisms during liquefaction, that might have caused grain-size segregation within dikes as the material is extruded, are shown. Symbols refer to Figure 9.

and Riccardo Civico (INGV, Rome, Italy) for opening the two trenches in the trial site of Mirabello.

REFERENCES

Amorosi, A., Pavesi, M., Ricci Lucchi, M., Sarti, G., and Piccin, A., 2008, Climatic signature of cyclic fluvial architecture from the Quaternary of the central Po Plain, Italy: Sedimentary Geology, v. 209, p. 58–68.

Amorosi, A., Bruno, L., Facciorusso, J., Piccin, A., and Sammartino, I., 2016, Stratigraphic control on earthquake-induced liquefaction: a case study from the Central Po Plain (Italy): Sedimentary Geology, v. 345, p. 42–53.

Amoroso, S., Milana, G., Rollins, K.M., et al., 2017, The first Italian blast-induced liquefaction test (Mirabello, Emilia-Romagna, Italy): description of the experiment and preliminary results: Annals of Geophysics, v. 60, no. S0556.

Andrew, D.C.A., and Martin, G.R., 2000, Criteria for liquefaction of silty soils: 12th World Conference on Earthquake Engineering: Auckland, New Zealand, Proceedings, Paper 0312.

Argnani, A., Fontana, D., Stefani, C., and Zuffa, G.G., 2006, Palaeogeography of the Upper Cretaceous–Eocene carbonate turbidites of the Northern Apennines from provenance studies: Geological Society of London, Journal, v. 262, p. 259–275.

Arribas, J., and Tortosa, A., 2003, Detrital modes in sedimenticlastic sands from first-order streams of the Iberian Range, Spain: the potential for sand generation of different sedimentary rocks: Sedimentary Geology, v. 159, p. 275–303.

Ashford, S., Rollins, K.M., and Lane, J., 2004, Blast-induced liquefaction for full-scale foundation testing: Journal of Geotechnical and Geoenvironmental Engineering, v. 130, p. 798–806.

ASTM D2487-11, 2011, Standard Practice for Classification of Soils for Engineering Purposes, Unified Soil Classification System.

Boccaletti, M., Bonini, M., Corti, G., Gasperini, P., Martelli, L., Piccardi, L., Severi, P., and Vannucci, G., 2004, Seismotectonic map of the Emilia-Romagna Region: Regione Emilia-Romagna, CNR, SELCA, Firenze.

Boncio, P., Amoroso, S., Vessia, G., Francescone, M., Nardone, M., Monaco, P., Famiani, D., Di Naccio, D., Mercuri, A., Manuel, M.R., Galadini, F., and Milana, G., 2018, Evaluation of liquefaction potential in an intermountain Quaternary lacustrine basin (Fucino basin, central Italy): Bulletin of Earthquake Engineering, v. 16, p. 91–111.

Bray, J., and Sancio R.B., 2006, Assessment of the liquefaction susceptibility of fine-grained soils: Journal of Geotechnical and Geoenvironmental Engineering, v. 132, p. 1165–1177.

Bray, J., Cubrinovski, M., Zupan, J., and Taylor, M., 2014, Liquefaction effects on buildings in the central business district of Christchurch: Earthq Spectra, v. 30, p. 85–109.

Caputo, R., and Papathanasiou, G., 2012, Ground failure and liquefaction phenomena triggered by the 20 May, 2012 Emilia-Romagna (Northern Italy) earthquake: case study of Sant'Agostino–San Carlo–Mirabello zone: Natural Hazards and Earth System Sciences, v. 12, p. 3177–3180.

Carminati, E., Doglioni, C., and Scrocca D., 2005, Magnitude and causes of long-term subsidence of the Po Plain and Venetian region, *in* Fletcher, C.A., and Spencer, T., Da Mosto, J., and Campostrini, P., eds., Flooding and Environmental Challenges for Venice and its Lagoon: State of Knowledge: Cambridge, UK, Cambridge University Press, p. 21–28.

Chang, W.J., Ni, S.H., Huang, A.B., Huang, Y.H., and Yang, Y.Z., 2011, Geotechnical reconnaissance and liquefaction analyses of a liquefaction site with silty fine sand in Southern Taiwan: Engineering Geology, v. 123, p. 235–245.

Chen, L., Hou, L., Cao, Z., Yuan, X., Sun, R., Wang, W., Mang, F., Chen, H., and Dong, L., 2008, Liquefaction investigation of Wenchuan earthquake: 14th World Conference on Earthquake Engineering, Beijing, China, Proceedings, S31–049.

Cobain, S.L., Hodgson, D.M., Peakall, J., and Shiers., M.N., 2017, An integrated model of clastic injectites and basin floor lobe complexes: implications for stratigraphic trap plays: Basin Research, v. 29, p. 816–835.

Di Felice, R., 2010, Liquid–solid suspension theory with reference to possible applications in geology: Basin Research, v. 22, p. 591–602.

Diggs, T.N., 2007, An outcrop study of clastic injection structures in the Carboniferous Tesnus Formation, Marathon Basin, Trans-Pecos Texas, *in* Hurst, A., and Cartwright, J., eds., Sand Injectites: Implications for Hydrocarbon Exploration and Production: American Association of Petroleum Geologists, Memoir, v. 87, p. 37–48.

Emergeo Working Group, 2013, Liquefaction phenomena associated with the Emilia earthquake sequence of May–June 2012 (Northern Italy): Natural Hazards and Earth System Sciences, v. 13, p. 935–947.

Figueroa, J.L., Saada, A.S., and Liang, L., 1995, Effect of the grain size on the energy per unit volume at the onset of liquefaction: 3rd International Conference on Recent Advances in Geotechnical Earthquake Engineering and Soil Dynamics, St. Louis, Missouri, Proceedings, v. 1, p. 197–202.

Fioravante, V., Giretti, D., Abate, G., et al., 2013, Earthquake geotechnical engineering aspects: the 2012 Emilia-Romagna earthquake (Italy): 7th International Conference on Case Histories in Geotechnical Engineering, Chicago, Illinois, Proceedings, p. 1–34.

Finno, R.J., Gallant, A.P., and Sabatini, P.J., 2016, Evaluating ground improvement after blast densification at the Oakridge landfill: Journal of Geotechnical and Geoenvironmental Engineering, v. 142, p. 1–13.

Fontana, D., 1991, Detrital carbonate grains as provenance indicators in the Upper Cretaceous Pietraforte Formation (northern Apennines): Sedimentology, v. 38, p. 1085–1095.

Fontana, D., Lugli, S., Marchetti Dori, S., Caputo, R., and Stefani, M., 2015, Sedimentology and composition of sands injected during the seismic crisis of May 2012 (Emilia, Italy): clues for source layer identification and liquefaction regime: Sedimentary Geology, v. 325, p. 158–167.

Garzanti, E., Vezzoli, G., and Andò, S., 2011, Paleogeographic and paleodrainage changes during Pleistocene glaciations (Po Plain, Northern Italy): Earth-Science Reviews, v. 105, p. 25–48.

Geotema, 2014, Microzonazione sismica livello 2 con locali approfondimenti di livello 3, del Comune di Mirabello (FE), Regione Emilia-Romagna: Relazione illustrativa e 7 tavv (in Italian).

Ghielmi, M., Minervini, M., Nini, C., Rogledi, S., and Rossi, M., 2013, Late Miocene e Middle Pleistocene sequences in the Po Plain–Northern Adriatic Sea (Italy): the stratigraphic record of modification phases affecting a complex foreland basin: Marine and Petroleum Geology, v. 42, p. 50–81.

Giona Bucci, M., Almond, P., Villamor, P., Ries, W., Smith, C., and Tuttle, M., 2017, When the earth blisters: exploring recurrent liquefaction features in the coastal system of Christchurch, New Zealand: Terra Nova, v. 29, p. 162–172.

Gohl, W.B., Martin, T., and Elliott, R.J., 2009, Explosive compaction of granular soils and in situ liquefaction testing using sequential detonation of explosives: International Symposium on Ground Improvement Technologies and Case Histories, Singapore, Geotechnical Society of Singapore, Proceedings, p. 199–207.

Hurst, A., Scott A., and Vigorito M., 2011, Physical characteristics of sand injectites: Earth-Science Reviews, v. 106, p. 215–246.

Kazerouni, A.M., Friis, H., Svendsen, J.B., and Weibel, R., 2011, Heavy mineral sorting in downwards injected Palaeocene sandstone, Siri Canyon, Danish North Sea: Sedimentary Geology, v. 236, p. 279–285.

Kishida, H., 1970, Characteristics of liquefaction of level sandy ground during the tokachioki earthquake: Soils and Foundations, v. 10, p. 103–111.

Kramer, S.L., 1996, Geotechnical Earthquake Engineering: Upper Saddle River, New Jersey, Prentice Hall, 653 p.

Krinitzsky, E.L., Chang, F.K., and Nuttli, O.W., 1988, Magnitude-related earthquake ground motions: Association of Engineering Geologists, Bulletin, v. 2, p. 399–423.

Idriss, I.M., and Boulanger, R.W., 2008, Soil Liquefaction during earthquakes: Earthquake Engineering Research Institute, Monograph MNO-12, 237 p.

Ishihara, K., 1984, Post-earthquake failure of a tailings dam due to liquefaction of the pond deposit: International Conference on Case Histories in Geotechnical Engineering: St. Louis, Missouri, Proceedings, v. 3, p. 1129–1143.

Ishihara, K., 1993, Liquefaction and flow failure during earthquakes: Geotechnique, v. 43, p. 351–415.

Lugli, S., Marchetti Dori, S., Fontana, D., and Panini, F., 2004, Composition of sands in cores along the high-speed rail (TAV): preliminary indications on the sedimentary evolution of the Modena plain: Alpine and Mediterranean Quaternary, v. 17, p. 379–389.

Lugli, S., Marchetti Dori, S., and Fontana, D., 2007, Alluvial sand composition as a tool to unravel the Late Quaternary sedimentation of the Modena plain, northern Italy, *in* Arribas, J., Critelli, S., and Johnsson, M.J., eds., Sedimentary Provenance and Petrogenesis: Perspectives from Petrography and Geochemistry: Geological Society of America, Special Paper 420, p. 57–72.

Marcuson, W.F., 1978, Definition of terms related to liquefaction: American Society of Civil Engineers, Journal of the Geotechnical Engineering Division, Proceedings, v. 104, p. 1197–1200.

Mariotti, G., and Doglioni, C., 2000, The dip of the foreland monocline in the Alps and Apennines: Earth and Planetary Science Letters, v. 181, p. 191–202.

Minarelli, L., Amoroso, S., Tarabusi, G., Stefani, M., and Pulelli, G., 2016, Down-hole geophysical characterization of middle–upper Quaternary sequences in the Apennine Foredeep, Mirabello, Italy: Annals of Geophysics, v. 59, no. S0543.

Mitchell, J.K., and Soga, K., 2005, Fundamentals of Soil Behavior, Third Edition: Hoboken, New Jersey, John Wiley and Sons, 558 p.

Mount, J.F., 1993, Formation of fluidization pipes during liquefaction: examples from the Uratanna Formation (Lower Cambrian), South Australia: Sedimentology, v. 40, p. 1027–1037.

Nichols, R.J., Sparks, R.S.J., and Wilson, C.J.N., 1994, Experimental studies of the fluidization of layered sediments and the formation of fluid escape structures: Sedimentology, v. 41, p. 233–253.

Owen, G., and Moretti, M., 2011, Identifying triggers for liquefaction-induced soft-sediment deformation in sands: Sedimentary Geology, v. 235, p. 141–147.

Passeri, F., Comina, C., Marangoni, V., Foti, S., and Amoroso S., 2018, Geophysical tests to monitor blast-induced liquefaction, the Mirabello (NE, Italy) test site: Journal of Environmental and Engineering Geophysics, v. 23, p. 319–333.

Pesci, A., Amoroso, S., Teza, G., and Minarelli, L., 2018, Characterisation of soil deformation due to blast-induced liquefaction by UAV-based photogrammetry and terrestrial laser scanning: International Journal of Remote Sensing, 20 p.

Quigley, M., Bastin, S., and Bradley, B., 2013, Recurrent liquefaction in Christchurch, New Zealand during the Canterbury earthquake sequence: Geology, v. 41, p. 419–422.

Ricci Lucchi F., 1986, The Oligocene to Recent foreland basins of the Northern Apennines, *in* Allen, P.A., and Homewood, P., eds., Foreland Basin: International Association of Sedimentologists, Special Publication 8, p. 105–139.

Rodríguez-Pascua, M.A., Silva, P.G., Perez-Lopez, R., Giner-Robles, J.L., Martín-Gonzalez, F., and Del Moral, B., 2015, Polygenetic sand volcanoes: on the features of liquefaction processes generated by a single event (2012 Emilia Romagna 5.9 M_w earthquake Italy): Quaternary International, v. 357, p. 329–335.

Rollins, K.M., Lane, J.D., Nicholson, P.G., and Rollins, R.E., 2004, Liquefaction hazard assessment using controlled blasting techniques: 11th International Conference on Soil Dynamics and Earthquake Engineering, Berkeley, California, Proceedings, v. 2, p. 630–637.

Ross, J.A., Peakall, J., and Keevil, G.M., 2011, An integrated model of extrusive sand injectites in cohesionless sediments: Sedimentology, v. 58, p. 1693–1715.

Ross, J.A., Peakall, J., and Keevil, G.M., 2013, Sub-aqueous sand extrusion dynamics: Geological Society of London, Journal, v. 170, p. 593–602.

Ross, J.A., Peakall, J., and Keevil, G.M., 2014, Facies and flow regimes of sandstone-hosted columnar intrusions: insights from the pipes of Kodachrome Basin State Park: Sedimentology, v. 61, p. 1764–1792.

Stefani, M., Minarelli, L., Fontana, A. and Hajdas, I., 2018, Regional deformation of Late Quaternary fluvial sediments in the Apennines foreland basin (Emilia, Italy): International Journal of Earth Sciences, 15 p.

Tokimatsu, K., and Yoshimi, Y., 1983, Empirical correlation of soil liquefaction based on SPT N-value and fines content: Soils and Foundations, v. 23, p. 56–74.

Weltje, G.J., and Von Eynatten, H., 2004, Quantitative provenance analysis of sediments: review and outlook: Sedimentary Geology, v. 171, p. 1–11.

Wentz, F.J., van Ballegooy, S., Rollins, K.M., Ashford, S.A., and Olsen, M.J., 2015, Large scale testing of shallow ground improvements using blast-induced liquefaction: 6th International Conference on Earthquake Geotechnical Engineering, Christchurch, New Zealand, Proceedings, 10 p.

Youd, T.L., and Perkins, D.M., 1978, Mapping liquefaction induced ground failure potential: American Society of Civil Engineers, Journal of the Geotechnical Engineering Division, Proceedings, v. 104, p. 443–446.

Zuffa, G.G., 1985, Optical analyses of arenites: influence of methodology on compositional results, *in* Zuffa, G., ed., Provenance of Arenites: Dordrecht, Netherlands, D. Reidel, NATO Advanced Study Institute, v. 148, p. 165–189.

Received 26 March 2018; accepted 19 October 2018.

Queries for sedp-88-12-04

This manuscript/text has been typeset from the submitted material. Please check this proof carefully to make sure there have been no font conversion errors or inadvertent formatting errors. Allen Press.